CHIRP SCALE PROCESSING FOR IMAGING SONAR

R.Sathishkumar, T.V.S.Prasad Gupta, M.Ajay Babu and Habibullakhan
Department of Electronics and Communication Engineering, KL University, India
Email:drsathishkmr@gmail.com

***Abstract*–Imaging the sea floor using high precision sonar is at the stage where the efficiency and robustness are of concern. Synthetic aperture sonar (SAS) has the appealing property of range and frequency independent spatial resolution. SAS data's are more challenging to process than the conventional counterparts, because the towfish is more complicated and usually non stationary. Time domain algorithms can handle general sonar, but they are inefficient. Several frequency domain algorithms have been modified to handle a limited number of SAS cases. In the present work, a closed form expression for the stripmap geometry model is mathematically derived and analyzed from the high resolution SAS imaging point of view. Further, we discussed the processing method for SAS data and proposed a chirp scaling algorithm (CSA). We have focused on the application of CSA processor that is based on the use of the Fourier transforms. The simulation results validate the analysis and the feasibility of this algorithm.**

Keywords: Sonar, Range Doppler, Chirp Scaling, Back Projection, ω-k Algorithm

I.INTRODUCTION

Side looking sonar (SLS) and synthetic aperture sonar (SAS) technologies provide high resolution imagery for mine countermeasure applications. While SLS has been well developed for several decades, SAS is a fairly new technology [1-5]. SLS systems use antenna arrays to scan the seabed in a narrow beam fashion. The reconstructed images present a resolution that is limited by the antenna aperture and that also decreases with range. SAS overcomes these limitations: a single antenna system moves along a straight line and pings are sent at different positions. Hence, a synthetic array, theoretically as long as desired, is built up and the resolution increases. Furthermore, the resolution is independent of the range [6]. The use of SAS is undergoing considerable growth in both the civilian and military domains in the discrimination, identification, and classification of targets. It has the ability to produce higher resolution images at lower frequencies allowing greater ranges to be achieved, while maintaining a constant cross range resolution as a function of range away from the sonar. Although the images produced on SAS systems often have a photograph like character, there are particular properties that demand fundamentally different interpretation than optical images [7]. Typically, a 100 kHz SAS would operate with 10-50 pings gives much better resolution than SLS. Synthetic aperture is sampled finer than half a wavelength and this constrains the along track speed and limits the area mapping rate. Thus, with a single transmitter and an array of hydrophones increases the area mapping rate. The azimuth resolution is the ratio between the acoustic wave length and the length of the array. The typical ratio is of the order 1:60-1:400 (resolution of 1 m at 60 and 400 m range, respectively). The theoretical azimuth resolution is half the length of each element in the receive array, at all ranges. In general, this resolution is not practically achievable, and the practical will be 1.5 – 2 times lower. The image formation aligning the echoes to less than 0.1 millimetres. This is made possible through broadband technology combined with adaptive focusing. In this work, the paper is arranged as follows. The imaging geometry and the signals are analyzed in Section II. An overview of time domain and frequency domain algorithm for this kind of system is discussed in Section III, where the chirp scaling function is highlighted. The system parameters and the simulation are discussed in Section IV. Finally, simulating results are shown in Section V to validate the analysis and the algorithm, and then, Section VI concludes this paper.

II. IMAGING GEOMETRY

Modern SAS systems provide an area coverage rate of several square kilometres per hour with centimetric resolution. In addition, when combined with depth estimation techniques which exploit two SAS arrays with a large vertical separation between them for high accuracy interferometry, SAS can deliver high quality 3D images of the seabed which are sufficient to meet the standards for hydrographic surveys today. The Figure.1 shows the geometry of the stripmap model.

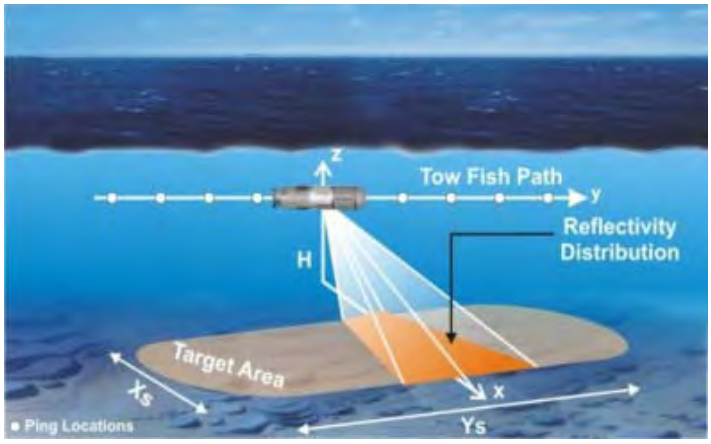

Figure.1 Geometry of stripmap SAS

Here, the image coordinate system is denoted (x,y), while the data collection coordinate system is denoted (t,u). Xs and Ys are the swath widths in range and along track, and H is the platform altitude. In this configuration the system maintains the same broadside radiation pattern throughout the data collection period. The SAS moves through the water in the y direction at an altitude z off the sea floor. The signal is sent out along the x, or ground range, axis. The complex reflectivity distribution of the target field is given by ff(x,y). The complex reflectivity distribution of the target field is given by ff(x,y). The raw echoes are

$$E(t,u) \approx \int_x \int_y ff(x,y).\,[a(t,x,y-u) *_t S_m(t-\frac{2}{c}\sqrt{x^2+(y-u)^2})]dxdy \quad (1)$$

The transmitted signal is contained in $S_m(t)$, and the time delay term describes the range migration of a target as the platform traverses the aperture. The LFM chirp signal is

$$S_m(t) = \mathrm{rect}(t/\tau_p)\exp(j(\omega_c t + \pi K t^2)) \quad (2)$$

Where ω_c is the carrier radial frequency, ω is the modulated range frequency variable, t is the temporal ordinate and K is the signal chirp rate. The chirped, demodulated raw data is along track Fourier transformed to form

$$E_b(t,k_v) = \sqrt{\pi\, x_0 c/j\omega_c}.\,\mathrm{rect}\,[\frac{t-2R_m(k_v;\,x_0)/c}{\tau_p}]\exp(j\pi K_{cr}(k_v;\,x_0).(t-2\,R_m(k_v;\,x_0)/c)^2]$$
$$\exp\,[-j\sqrt{(2\omega_c/c)^2-k_v^2}\;.\;x_0] \quad (3)$$

where K_{cr} is the k_v dependent chirp rate

$$K_{cr}\,(k_v;\,x_0) = \frac{c^2 K[(2\omega_c/c)^2-k_v^2]3/2}{1-8\pi\, x_0 K_c\; k_v^2}$$

and R_m is the range migration through k_u space and

$$R_m\,(k_u;\,x_0) = \frac{x_0}{\sqrt{1-\left(\frac{k_v}{2\omega_c/c}\right)^2}}$$

$$\text{Hence } C_f(k_v) = \left[1-\left(\frac{k_v}{2\omega_c/c}\right)^2\right]^{-1/2}-1 \quad (4)$$

describes the spatial wave number dependent part of the signal trajectory, and the time locus of the reference range is given by

$$t_r(k_v) = \frac{2r_0}{c}\left(1+C_f(k_v)\right) \quad (5)$$

The range Fourier transform is

$$E_{cl}(\omega_b,k_v) = \sqrt{\pi\, x_0 c/\omega K_c}\;\;\mathrm{rect}\,[\frac{\omega_b}{2\pi r K_{cr}(k_v;r)(1+C_f(k_v))}] \quad (6)$$

where the interpretation of each phase term is shown to the left of the equation. The data is then windowed across the processing bandwidths and inverse Fourier transformed in range, forming

$$C_p(t,k_v) = \frac{\sqrt{\pi\, x_0 c}}{\omega_c}\,\mathrm{rect}\,(\frac{k_v}{B_{AT}})\,\frac{B_e}{\sqrt{K_c}}\,[\mathrm{sinc}[B_e(t-2\,x_0/c)].$$
$$\exp[-j(\sqrt{(2\omega_c/c)^2-k_v^2}\;-2\,\omega_c/c)\;x_0]\;\exp(j\,(k_v;r_0)-\;j2\frac{x_0\omega_c}{c}) \quad (7)$$

where the range and alongtrack processing bandwidths are Be and B_{AT}, respectively. The Figure.2 shows the base banded data in time and frequency domains.

III.IMAGING ALGORITHM

Synthetic aperture image reconstruction is an inverse problem. SAS traditionally involves the coherent processing scattering information from acoustic targets. Following data reception, a variety of methods in the Fourier or time domain may be used to construct images. For certain targets, resonances and elastic effects can interfere with the specular portions of backscattered echoes. The time delay associated with elastic or resonant responses destroys the uniqueness of the location to which the signal is mapped, and occasionally these resonant features can be mapped directly on top of target specular features, causing destructive interference and reduced image clarity. Destructive interference can be reduced and image clarity enhanced by incoherently summing separate images generated from sub apertures of SAS data. Additionally, limiting the aperture and frequency band of the pre processed data before applying an imaging algorithm is an effective method for understanding and localizing various elastic and non elastic target responses.

In Time Domain, Correlation Algorithm (CA) correlates the echo data against a model for the data that would have been received for each image pixel and records the peak value [8]. It is mathematically identical to delay and sum beamforming and back projection that can work with all array geometries. The downside is the computation time required to reconstruct a typical scene. Back projection algorithm (BPA) enables perfect image reconstruction for any trajectory or array configuration as long as there is a good estimate of the bottom topography [9]. It is computationally intensive, that led to the development of approximations to the beamforming techniques to reduce the computational load, so the algorithms could be loaded into a chip on the vehicle and can be processed in real time. The gain in computational time comes at the expensive of a degraded image. Fast Factorization Back projection (FFBP) is a recursive partitioning of the back projection integral, adapted from medical imaging and SAR, is a phase preserving inversion method and it is more sensitive to motion error [10]. Its usefulness is in the ability to scan a large area in less time than conventional methods with the ability to pick out targets that can be reprocessed at a higher resolution.

In FFBP the computation is conducted on a pulse by pulse basis allowing for parallel processing of the above equation. The carrier phase is removed by base banding then the signal is up sampled prior to using the principle of stationary phase for integration. It divides the full synthetic aperture into sub apertures and produces image for each sub aperture. While substantially faster than standard back projection, there is uncertainty whether FFBP produce any useful gain in speed or accuracy compared to Fourier methods. The main advantage is it can reconstruct images in real time on standard workstation with specialized parallel computers or field programmable gate arrays (FPGAs). Analysis of SAS imagery is based on the location of the target. So, it becomes important to move to the spatial domain [11]. Hence, in Frequency Domain, ω-k or Wave number (Seismic Migration or Range Migration) algorithm, compute fast Fourier transforms (FFTs). It starts with a 2D Fourier transform of the echo data into the wave number domain followed by a coordinate mapping and a phase amplitude correction [12]. It has faster processing times, at the expense of image degradation. ω-k along with Range Doppler algorithm (RDA) is mostly used in the SAR community. In practice, the wave number data is windowed to control the side lobe level of the reconstructed image. It handles the range dependence of the range azimuth coupling correctly, which gives it the ability to process data acquired over wide azimuth apertures. This is because the data are processed entirely in the two dimensional frequency domain, where the approximations used in the CSA and RDA is not needed. The Figure.3 shows the algorithm steps of RDA, CSA and ω-k. However, some approximations have to be made, notably the constant velocity assumption, which makes their error properties different from the RDA. Range Doppler algorithm (RDA) is computationally efficient and is phase preserving [13]. It is the most widely used algorithm because of its favorable tradeoff between efficiency, accuracy, maturity, and ease of implementation. It is designed for continuously collected data and can process the full azimuth bandwidth.

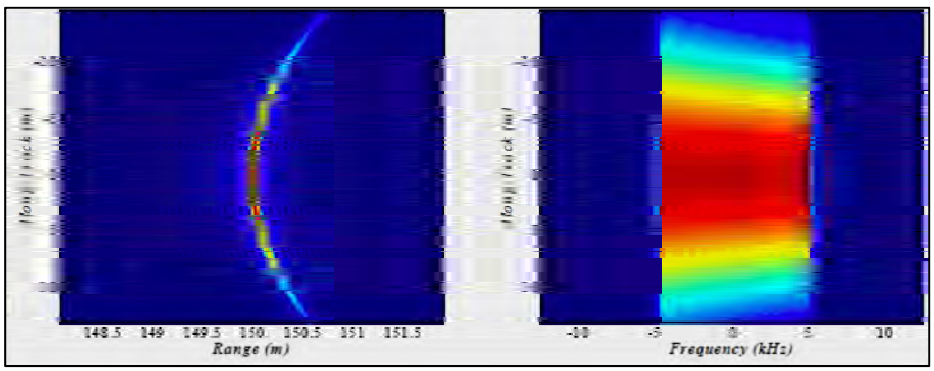

Figure.2 Baseband data (a) Time Domain (b) Frequency Domain

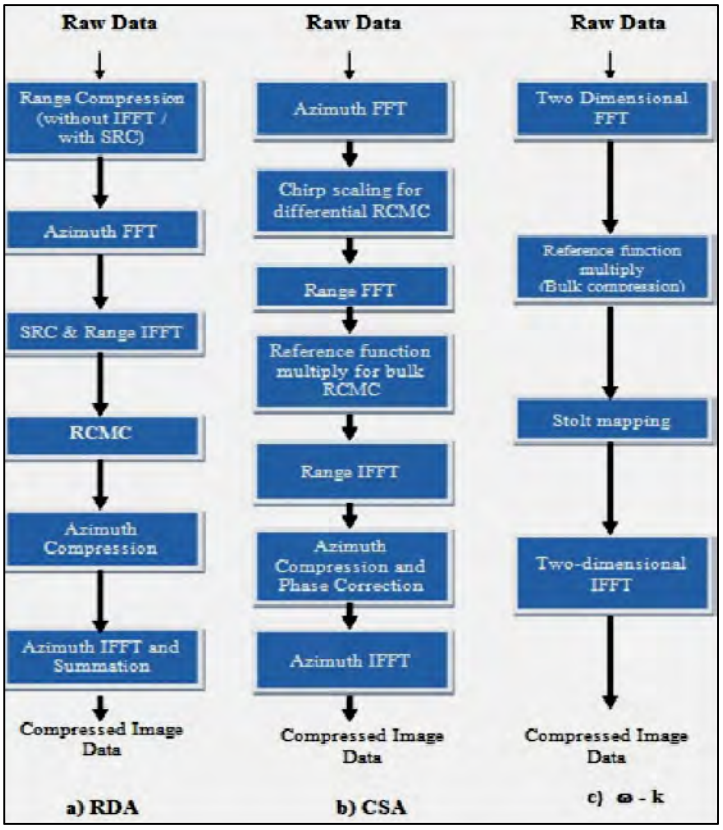

Figure.3 Algorithm steps of a) RDA b) CSA c) ω-k

It requires knowledge of the transmitted pulse for range compression and of the imaging geometry such as the range and towfish velocity for construction of the azimuth matched filter. It uses the large difference in time scale of range and azimuth data and approximately separates processing in these two directions using Range Cell Migration (RCM) correction. The time consuming computation in RDA and ω-k algorithms are the interpolation. Chirp Scaling Algorithm (CSA) is a good choice because it preserves the phase [14-15]. It requires the transmit signal to be a LFM chirp and uses a sequence of 2D phase multiplications and 2 D FFTs to reconstruct an image. It precompute full size complex arrays in addition to the input data array and the output image array. It is a method of curvature equalization where no grid interpolation is required. After wavenumber transformation, the range migration trajectories have been adjusted to have congruent loci, equivalent to the trajectory at a selected reference range. Pulse compression, including secondary range compression, bulk range migration correction, deconvolution of the frequency dependent amplitude term and windowing are performed across the bandwidth.

IV. SIMULATION

At sea, experiments are expensive. So models of the acoustic environment and the parameters are used to probe the performance limits of the sonar. The Figure.4 shows the SAS processing chain. Software tools such as Shallow Water Acoustic Tools (SWAT) do exist but have restricted availability and it can be difficult for users to determine the internal workings of the models used in the program. Many simple models just assume that the targets and seafloor are a cloud of point reflectors where each point reflector that comprises the seafloor is visible from all aspect angles within the physical beamwidth of the sonar. A faster approach to model realistic SAS imagery is to just model the scattering from the desired targets of interest and to superimpose these on real SAS data. In the SAS processing, the time domain methods can focus the data well but it is paid for by a huge computational cost. The BPA [16] can serve most cases, but its low efficiency makes it not a good choice. The efficiency of processing can be highly improved by performing the focusing in the frequency domain. CSA [17] is widely used in SAR imaging for its high efficiency and good precision. Wong and Yeo [18] pointed out that, if the RCM can be considered as unchangeable with azimuth, the CSA can be used to identify the azimuth FM rates within the same range.

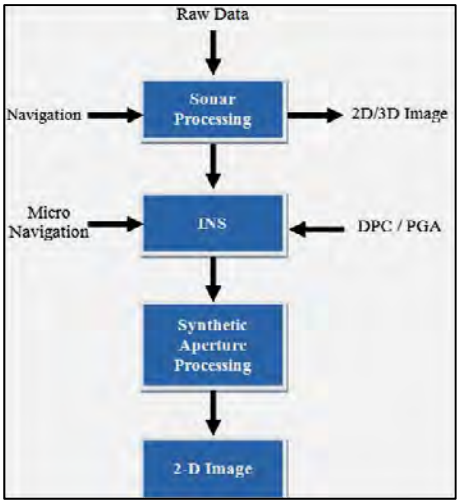

Figure.4 SAS Processing Chain

To facilitate the application of CSA, the range variant and range invariant terms are expanded as a series in terms of the range frequency. In this algorithm, a CS procedure is used to equalize the RCMs of the different range cells, and then, a bulk RCM correction operation is used to correct the RCMs of the entire target field.In the present work, we carried out the processing in the MATLAB and simulate the LFM down Chirp signal for the duration of 150 msec .The signal bandwidth is 20 kHz and the center frequency is 30 kHz. We assume the receiver width for 22 cm. The range resolution is 5 cm and the along track resolution is15 cm. The propagation speed is 1500 m/sec and the sampling frequency is 15 kHz.

V. RESULTS AND DISCUSSIONS

Simulated images were focused using the ω-k and CSA. These algorithms are capable of diffraction limited imagery, but the accuracy is dependent upon the range extent of the image. Seven point targets were generated and focused over a range of 30 m, as shown in the Figure.5 that contains the output of the CSA and ω-k algorithm using (linear Stolt interpolation). Each algorithm used 100 m as the reference range. As the range is increased to 130 m, these effects are quite noticeable: the response due to CSA is significantly attenuated and the sidelobe structure is completely degraded. It is apparent that as the processing complexity of the ω-k algorithm is increased, so is the accuracy, as expected. The assertion thus far has been that CSA should theoretically outperform ω-k based on the assumption that the interpolation step requires much computational complexity in order to attain an adequate image quality. This result confirms that the ω-k algorithm actually attains good image quality with the use of simple linear Stolt interpolation and time domain zero padding. In terms of processing requirements, the CSA algorithm images displayed main lobe attenuation more quickly than the ω-k processed images. Thus, based on these tests, CSA algorithm should be the image processor for this system. The Figure.5 shows the images obtained by CSA and ω-k Algorithm processing.

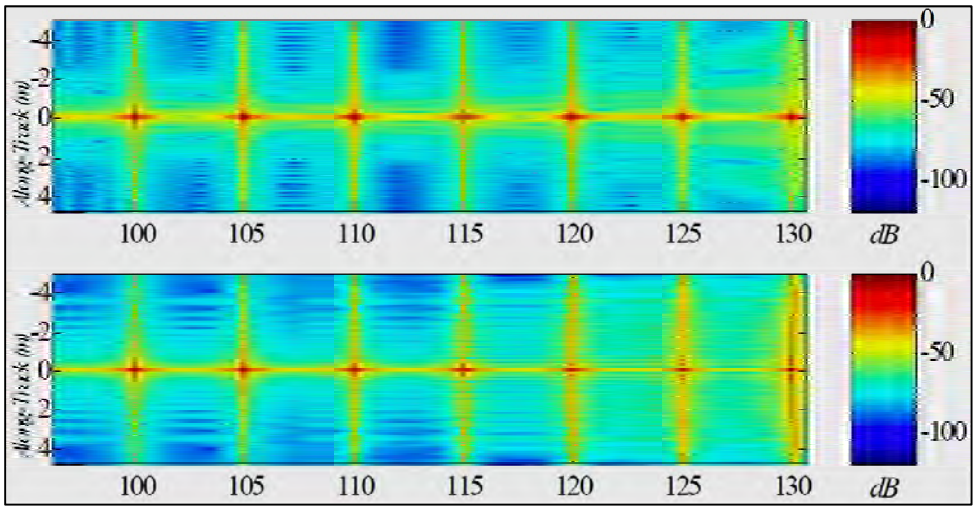

Figure.5 Focused Image of seven point targets CSA (Top) and ω-k Algorithm (Bottom)

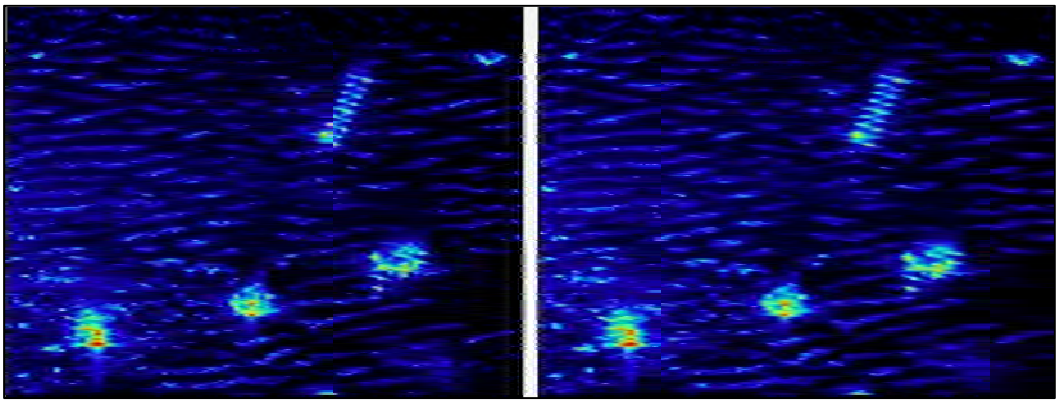

Figure.5 Images obtained by CSA (Left) and ω-k Algorithm (Right)

VI. CONCLUSION

For high resolution stripmap SAS, there are azimuth dependence component of RCM and the quadratic phase after linear RCM correction. In this work, the azimuth CSA has been used to correct the azimuth dependence component of RCM and the quadratic phase in the range frequency domain. Then, we performed a chirp scaling along the range to correct the range dependence component. Finally, we have presented some simulations to illustrate the efficiency of the proposed algorithm. The simulation results about the imaging quality and the phase behavior validate the feasibility of the imaging algorithm and the correctness of the analysis. All of the approximations are valid based on the special precondition. Therefore, when applying the CSA algorithm for the real SAS data imaging, especially in the long wavelength, an evaluation on the validity of the preconditions should be first carried out according to specific parameters. The evaluation can help users to determine the reasonable approximations in algorithm derivation and can make sure that all of the approximations are valid and accurate.

ACKNOWLEDGMENT

We are grateful to the management of the KL University for providing the necessary facilities for the stimulating research environment. We received continual encouragement from Prof.Dr.Shree Hari Rao, Vice Chancellor of the KL University. We received a lot of guidance from Dr.Dhilsha Rajappan, Joint Project Director of National Institute of Ocean Technology–NIOT, India, who provided us the initial desire, interest and ideas on ocean engineering projects. We extend our thanks to Prof.N.Venkatram, Dean of Electrical Sciences of, KL University for his continual encouragement on the research work.

REFERENCES

[1] Bruce, M.P.; , "A processing requirement and resolution capability comparison of side-scan and synthetic-aperture sonars," IEEE Journal of Oceanic Engineering, vol.17, no.1, pp.106-117, Jan 1992
[2] Key, W.H.; , "Side scan sonar technology," IEEE Conference OCEANS-2000, vol.2, no., pp.1029-1033 vol.2, 2000
[3] Coiras, E.; Petillot, Y.; Lane, D.M.; , "Multiresolution 3-D Reconstruction From Side-Scan Sonar Images," IEEE Transactions on Image Processing, vol.16, no.2, pp.382-390, Feb. 2007
[4] Langner, F.; Knauer, C.; Jans, W.; Ebert, A.; , "Side scan sonar image resolution and automatic object detection, classification and identification," IEEE OCEANS 2009-EUROPE , vol.1, no.1, pp.1-8, 11-14 May 2009
[5] M. P. Hayes, "Synthetic aperture sonar: A review of current status," IEEE Journal of Oceanic Engineering, vol. 34, no. 3, pp. 207–223, July 2009.
[6] Raquel Fandos and Abdelhak M. Zoubir, "Optimal Feature Set for Automatic Detection and Classification of Underwater Objects in SAS Images", IEEE Journal of Selected Topics in Signal Processing, vol. 5, no. 3, pp 454-468, June 2011
[7] Anthony P. Lyons, Douglas A. Abraham, and Shawn F. Johnson, "Modeling the Effect of Seafloor Ripples on Synthetic Aperture Sonar Speckle Statistics", IEEE Journal of Oceanic Engineering, vol. 35, no. 2, pp 242–249, April 2010
[8] Chialin Wu; Liu, K.Y.; Jin, M.; , "Modeling and a Correlation Algorithm for Spaceborne SAR Signals,", IEEE Transactions on Aerospace and Electronic Systems, vol.AES-18, no.5, pp.563-575, September 1982
[9] Desai, M.D.; Jenkins, W.K.; , "Convolution backprojection image reconstruction for spotlight mode synthetic aperture radar," IEEE Transactions on Image Processing, vol.1, no.4, pp.505-517, October 1992
[10] Shippey, G.; Banks, S.; Pihl, J.; , "SAS image reconstruction using Fast Polar Back Projection: comparisons with Fast Factored Back Projection and Fourier-domain imaging," Oceans 2005-Europe , vol.1, no., pp. 96- 101 Vol. 1, 20-23 June 2005
[11] Stepinski, T.; , "An Implementation of Synthetic Aperture Focusing Technique in Frequency Domain," Ultrasonics, IEEE Transactions on Ferroelectrics and Frequency Control, vol.54, no.7, pp.1399-1408, July 2007
[12] Hee-Sub Shin; Jong-Tae Lim; , "Omega-k Algorithm for Airborne Forward-Looking Bistatic Spotlight SAR Imaging," IEEE Transactions on Geosciences and Remote Sensing Letters, , vol.6, no.2, pp.312-316, April 2009
[13] Yew Lam Neo; Wong, F.H.; Cumming, I.G.; , "Processing of Azimuth-Invariant Bistatic SAR Data Using the Range Doppler Algorithm," IEEE Transactions on Geoscience and Remote Sensing, vol.46, no.1, pp.14-21, January 2008
[14] Gough, P.T.; Hawkins, D.W.; , "Imaging algorithms for a strip-map synthetic aperture sonar: minimizing the effects of aperture errors and aperture undersampling," IEEE Journal of Oceanic Engineering, vol.22, no.1, pp.27-39, January 1997

[15] Kargl, S.G.; Williams, K.L.; Thorsos, E.I.; , "Synthetic Aperture Sonar Imaging of Simple Finite Targets," IEEE Journal of Oceanic Engineering, vol.37, no.3, pp.516-532, July 2012
[16] J. Sanz-Marcos, J. J. Mallorqui, and A. Broquetas, “Bistatic parasitic SAR processor evaluation,” in Proc. IGARSS, 2004, vol. 6, pp. 3666–3669.
[17] R. K. Raney, H. Runge, I. G. Cumming, R. Bamler, and F. H. Wong, “Precision of SAR processing using chirp scaling,” IEEE Transactions on Geosciences and Remote Sensing, vol. 32, no. 4, pp. 786–799, July 1994.
[18] F. H. Wong and T. Yeo, “New application of nonlinear chirp scaling in SAR data processing,” IEEE Transactions on Geosciences and Remote Sensing, vol. 39, no. 5, pp. 946–953, May 2001.